Atomic and electronic structure and interatomic potentials at a polar ceramic/metal interface: {222}MgO/Cu

R. Benedek and D. N. Seidman
Materials Science and Engineering Department, Northwestern University, Evanston, Illinois 60208

M. Minkoff
Mathematics and Computer Science Division, Argonne National Laboratory, Argonne, Illinois 60439

L. H. Yang
Condensed Matter Physics Division, Lawrence Livermore National Laboratory, University of California, Livermore, California 94551

A. Alavi
School of Mathematics and Physics, The Queen's University of Belfast, Belfast BT7 1NN, Northern Ireland
(Received 7 June 1999)

Local density functional theory (LDFT) calculations, within the plane-wave-pseudopotential framework, are performed for the {222}MgO/Cu polar interface, with the objective of elucidating the atomic and electronic structure of the interface, as well as interface interatomic potentials. Calculations are performed for both coherent interfaces and semicoherent interfaces that approximate the lattice constant mismatch of the true system. Calculations of local electronic density of states and adhesive energies are performed primarily for coherent interfaces. The density of electronic states at the interface for the oxygen-terminated configuration exhibits a peak in the bulk MgO energy gap that results from O($2p$)-Cu($3d$) hybridization. The calculated interface adhesive energies for coherent interfaces as a function of the interface spacing and translation state are well reproduced by a simple analytical expression that combines an attractive Rydberg-function term and a repulsive pairwise Born-Mayer potential across the interface. Calculations are performed for a semicoherent interface with 5×5 Cu layer unit cells opposite 4×4 MgO layer unit cells, an approximation to the true system with lattice constant ratio of 7/6, to investigate the relaxation at the interface in the presence of misfit. The terminating oxygen layer as well as the interface Cu layer exhibits warping albeit on a scale of less than 0.1 Å. [S0163-1829(99)12047-2]

I. INTRODUCTION

Interfaces between ceramic and metallic phases are a prominent feature in many technologically important materials,[1,2] and understanding their structure and properties is therefore of considerable interest. Recently, atomic-scale structural characterization of some relatively simple ceramic/metal (C/M) interfaces such as {100}MgO/Ag,[3–5] {222}MgO/Cu,[6–9] {222}CdO/Ag,[10] alumina/Cu,[11] spinel/Ag and Al,[12] and alumina/Nb (Ref. 13) has been made by electron[14] and field-ion microscopy and by x-ray techniques. Realistic atomistic simulations of such systems are desirable in order to elucidate the experimental observations and to address features inaccessible to experiment. The lack of interface interatomic potentials of demonstrated reliability, however, has been an obstacle to the application of classical (molecular statics and dynamics and Monte Carlo) simulations to ceramic/metal interfaces. First-principles calculations appear indispensable for improving our theoretical understanding of C/M interfaces and also for providing benchmark results against which candidate interface interatomic potentials can be tested.

In this work, local density functional theory (LDFT) calculations are performed for {222}MgO/Cu, one of the most widely experimentally studied model C/M interfaces. Structurally and chemically sharp {222}MgO/Cu interfaces can be synthesized conveniently by internal oxidation.[6] The interfaces between MgO precipitates and the Cu matrix in internally oxidized specimens have been observed by atom-probe field ion microscopy[6,7] and high-resolution electron microscopy.[8,9] More recently, *Z*-contrast scanning transmission electron microscopy,[15] as well as spatially resolved electron energy loss spectroscopy[16,17] has been applied. MgO precipitates of octahedral shape with {222} facets are found primarily,[6] terminated by an oxygen layer at the interface.[18]

Simulation of {222}MgO/Cu is technically challenging because of its polarity (the atomic layers are charged on the ceramic side of the interface) and its high degree of misfit (about 15%). Unlike neutral interfaces [e.g., MgO/Pd(100)],[19] which have relatively weak adhesion, the chemical bonding of polar interfaces is typically strong. Because of the large misfit of {222}MgO/Cu, calculations for coherent interfaces must be regarded only as a preliminary step toward treating the full misfitting system. The ratio of MgO and Cu lattice constants is approximately 7/6, and therefore the periodic structures with the smallest interface unit cells are expected to contain at least 49 Cu atoms and 36 O (or Mg) atoms per (111) atomic layer. We have not yet done calculations on systems of this size (with at least several hundred atoms in the three-dimensional unit cells) but have instead treated smaller cells to elucidate the structure of the interface with misfit. In one calculation we consider a 4/3

 ©1999 The American Physical Society

ratio of Cu/O atomic spacing in one direction and equal spacing in the other; in a larger calculation we consider a lattice constant ratio of 5/4 (rather than 7/6) in both directions within the interface plane.

In previous work,[20] we calculated adhesive energies with LDFT for several MgO/Cu interfaces, within the coherent interface approximation; the Cu interatomic spacing parallel to the interface was scaled to match that of MgO. Larger adhesive energies were found for {222} than for {100} interfaces, and for the O-terminated than for the Mg-terminated {222} interface.

In the remainder of this introduction, we briefly review the literature on ceramic/metal interface interactions. Although polar interfaces, the focus of this work, are the most demanding case, we also mention models of nonpolar interfaces. A unified model suitable for treating interfaces of arbitrary orientation would, of course, be desirable. No comparisons of first-principles calculations with the atomistic models described below for polar interfaces have appeared in the literature.

Noguera and Bordier[21] present a qualitative discussion of the different contributions to the adhesion of nonpolar insulator-metal interfaces. Their Green's function formulation of insulator-metal interface electronic structure,[22] however, was designed to illustrate general spectral features, rather than to make quantitative predictions for real interfaces. A treatment of interface dispersion (van der Waals) forces based on the Lifshitz model has been performed for various metal-alumina interfaces;[23] however, this term represents only one component of the overall interaction in most systems, and furthermore, the accuracy of the results is difficult to assess. Image-charge interactions are thought to be significant for many C/M interfaces. An early formulation of image forces treated the metal as a continuum;[24,25] however, a discrete version[26] was recently applied successfully to {100}MgO/Ag interfaces.[27] The semiclassical aspect of the image-interaction approach may restrict its validity. The embedded-atom method (EAM) and approaches similar in spirit have been widely applied to metals, and a modified form (MEAM) has been introduced to treat systems with angular-dependent bonding. MEAM has been applied to alumina-aluminum interfaces.[28] An attractive feature of MEAM is that the interface interaction for native oxides is implicit in the potential models that describe the bulk metal and ceramic. Further, the model encompasses interfaces of arbitrary orientation within a single framework. Another treatment in which the interface interaction is implicit in the parametrization of the bulk energies is the variable charge ES+ potential model.[29] We note also that in the absence of potential models of demonstrated reliability for polar interfaces, *ad hoc* interface interaction potentials scaled to give the correct misfit but otherwise arbitrary[30] have also been applied.

In Sec. II, previous atomistic treatments of the interaction energy of ceramic/metal interface are reviewed. The precise reliability of most of these models is uncertain, particularly for polar interfaces. The method employed in our LDFT interface calculations is summarized in Sec. III. The application of LDFT to coherent and semicoherent {222}MgO/Cu interfaces is described in Sec. IV. The nature of the interface electronic structure is discussed.

II. LOCAL DENSITY FUNCTIONAL THEORY METHOD

In this work, the Kohn-Sham equations of LDFT[31] are solved within the plane-wave-pseudopotential representation.[32] Two different plane wave codes are used,[33,34] both of which employ iterative algorithms. A parallel code[34] was employed for the largest cells, as well as for the investigation of gradient corrections. Norm-conserving pseudopotentials[35] cast in the separable form of Kleinman and Bylander are used in conjunction with Gaussian-broadened energy levels[36] and special *k*-point[37] sampling. Most of the pseudopotentials are generated with the code of Troullier and Martins.[35]

The periodic unit cells in our calculations are based on either a multilayer or a periodic slab geometry.[20] The multilayer geometry[38,39] contains two interfaces per unit cell and an odd number of ceramic layers. The periodic slab geometry contains one C/M interface and two free surfaces separated by a gap. In our previous work,[20] substantially the same results for the interface adhesive energy were found for both geometries. The multilayer geometry, which is the preferable one because it avoids possible spurious electric fields that may occur in the periodic slab geometry, is restricted to coherent interfaces and translation states for which the two interfaces in the unit cell are identical.

Periodic boundary conditions restrict the calculations to commensurate interfaces. Most of the calculations treat the interface as coherent, with the in-plane Cu interatomic spacings stretched to the value for MgO. In Sec. III C, calculations for commensurate but semicoherent interfaces are presented, to determine the atomic-density dependence of the interface potential. Several stacking sequences of {222} (or {111}) coherent layers across the interface come into consideration. The ''normal'' sequence in which the ceramic (metal) sequence is continued across the interface, for example, *ABCabc*, where the upper-case letters refer to the stacking of the terminating species on the ceramic side (i.e., O when layers of that species are at the interface with Cu) and the lower-case refers to the metallic layers, is adopted throughout.

Gradient corrections to LDFT have recently been applied in a context similar to the present application, specifically, metal adsorbates on MgO{100}.[40] Binding energies were found substantially reduced relative to the uncorrected results. Experience suggests that gradient corrections improve accuracy in calculations for surfaces and adsorbates. Less experience exists regarding their application to heterophase interfaces. We present some calculations including the generalized gradient correction[41] (GGA) of adhesive energies to compare with LDFT calculations. Calculations pertaining to the comparison of the GGA with LDFT were done with the FEMD code.[34]

III. COHERENT INTERFACES

The MgO/Cu interface is known to be semicoherent, with a two-dimensional network of misfit dislocations. In spite of the large misfit, a substantial fraction of the interface, outside of the dislocation cores, is approximately coherent. Calculations for the coherent interface therefore give information about the coherent patches of the real interface. Another motivation for considering coherent interfaces is that properties

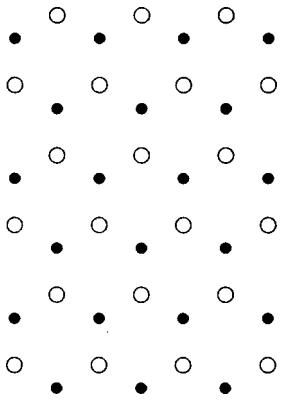

FIG. 1. Schematic illustration of interface-layer Cu atoms (filled circles) and O atoms (open circles) projected onto a plane parallel to the {111} layers for an oxygen terminated coherent MgO/Cu interface bilayer with parallel translation corresponding to the hollow position.

of the semicoherent interface may be approximated by weighted averages of properties of coherent interfaces that differ in their parallel translation.

A. Adhesive energy

1. Dependence on interface spacing

Although not measurable directly, the adhesive-energy curve is a useful construct for theoretical treatments of interface bonding. A possible ambiguity arises for polar interfaces, because the ceramic polar free surface may reconstruct. Our calculations[42] for MgO suggest that unreconstructed oxygen terminated {222}MgO free surfaces are metastable, although experimentally they are known to reconstruct.[43] Our calculated adhesive energies are with respect to unreconstructed ceramic free surfaces.

The total energy versus interface separation is calculated for anion- and cation-terminated {222}MgO/Cu interfaces, with the spacings between adjacent anion and cation (222) layers in MgO and (111) layers in Cu fixed at their bulk values, and, as noted above, the in-plane Cu interatomic spacings stretched to match the O interatomic spacing in bulk MgO, based on an assumed lattice constant, $a = 4.20$ Å. Two additional degrees of freedom to those already specified correspond to the rigid-body translation parallel to the interface of the Cu block relative to the MgO block of atoms. The minimum-energy translation state occurs at the hollow position, for which Cu atoms are equidistant from three nearest-neighbor terminating-plane-oxide atoms. The geometry of the interface bilayer corresponding to the hollow position is illustrated in Fig. 1, which shows schematically the locations of interface-layer Cu atoms (filled circles) and O atoms (open circles) projected onto a plane parallel to the layers. The energy variation as a function of (lateral) displacement from the hollow position is addressed below.

To reduce the computational effort, most of the adhesive energy calculations employ the periodic slab geometry, with (3,3|3) (Mg,O|Cu) layers in the *ABCabc* stacking sequence, and three special *k*-point (minimal) sampling. Tests for (5,5|5) layer cells, with 3 *k* points and 37 *k* points, yielded similar results. A gap of 6.2 Å between the slabs was employed in all of the periodic-slab calculations.

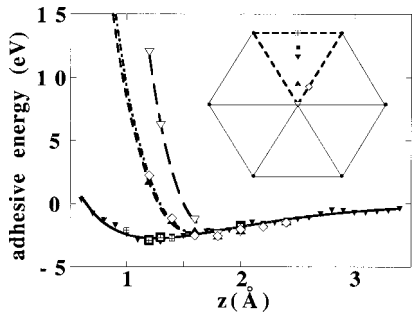

FIG. 2. Calculated energies per interface Cu atom of oxygen-terminated coherent {222}MgO/Cu interfaces versus interface separation for several parallel interface-translation states. The different symbols correspond to different translation states, which are illustrated in the inset. The symbol positions in the inset denote the location of the Cu interface layer atoms (projected onto a plane parallel to the interface) relative to the oxygen interface layer atoms, which are taken to be located at the vertices of the inset figure. Continuous curves represent fits based on the analytical model, Eq. (2). In this work, all of the hollow-centered triangles in the inset are regarded as equivalent, and the difference between fcc and hcp stacking at the interface is neglected.

The adhesive energy curve for nonpolar ceramic/metal interfaces (e.g., {100}MgO/Ag) was previously found to be well described by the Rydberg function[44,45]

$$E_r(z) = -\epsilon(1+z^*)\exp(-z^*), \tag{1}$$

where ϵ is the depth of the potential well, $z^* = (z - z_0)/l$, z_0 is the equilibrium interface separation, and l is a scaling length. We find the Rydberg function also provides an accurate fit to the adhesive energy of polar {222}MgO/Cu interfaces. From calculations at 0.1 Å intervals of z for a slab with (3,3|3) (Mg,O|Cu) layers, we obtain a prefactor $\epsilon = 2.75$ eV/atom, $z_0 = 1.25$ Å, and $l = 0.62$ Å for the O termination, and $\epsilon = 1.7$ eV/atom, $z_0 = 2.1$ Å, and $l = 0.86$ Å for the Mg termination. GGA calculations were performed for the oxygen-terminated interface. The interface spacing z_0 increases by about 0.08 Å, ϵ is reduced by 23% and l is reduced by 10%, in the GGA calculations relative to LDFT values. The correction introduced by the GGA in this context is relatively smaller than for adsorbed atoms on neutral substrates.[40]

The Cu-O bond length that corresponds to $z_0 = 1.25$ Å is about 2.1 Å. This is smaller than the sum of Cu and O ionic radii (about 2.3 Å), but larger than measured Cu-O bond lengths in other systems, as discussed below.

2. Dependence on parallel translation

LDFT total-energy calculations are performed on coherent interfaces for which the parallel translation vector of the interface as well as the interface separation is allowed to vary. Adhesive energy curves for O-terminated {222}MgO/Cu interfaces with different parallel translations of the Cu layers relative to the O interface layer are shown in Fig. 2. The parallel translation for each curve is indicated by the corresponding symbol in the inset diagram; results for the hollow position described in the preceding section corre-

spond to the inverted solid triangles. The other curves correspond to parallel translations, where the Cu atoms are displaced from the hollow position. Five different off-center positions are indicated in the inset, and the corresponding results for total energy are plotted. We note that all of the curves essentially coincide at large interface separation, but the curves for off-center positions deviate from the hollow-position curve at smaller interface separations. Thus the hollow-position curve gives an envelope that represents a lower bound for the off-center curves.

3. Analytical representation

The numerical results for varying interface spacing and parallel translation can be represented by a simple analytical form. A central force interaction complemented by a one-body z-dependent potential,

$$E_{\rm int}=E_1+E_2, \tag{2}$$

accurately reproduces the calculated adhesive energies. The one-body contribution $E_1=E_r(z)$, and the two-body term $E_2=\Sigma E_{\rm BM}\equiv\Sigma A\exp(-br_{ij})$ is a Born-Mayer-like interaction between pairs of Cu and O atoms across the interface. The quantity z_i is the distance of Cu atoms from the terminating insulating layer (assumed flat), and r_{ij} is the separation of Cu-O pairs. It is convenient to impose a cutoff on both E_1 and E_2, which we take to be of the Tersoff form.[46] We choose the cutoff parameters[46] $R=2.9$ Å and 1.6 Å for contributions to E_1 and E_2, respectively; the width of the Tersoff cutoff function in both cases is $D=0.3$ Å. The values obtained for the O termination are $A=4254$ eV, $b=4.73$ Å^{-1} and for the Mg termination $A=895$ eV, $b=3.54$ Å^{-1}. The continuous curves in Fig. 2 show the predictions of Eq. (2) for the O-terminated {222}MgO/Cu interface. Close agreement exists between the model and the LDFT total energy calculations.

The Mg-terminated {222}MgO/Cu interfaces have not been observed experimentally, and our further considerations will, therefore, refer only to the O termination. Since the equilibrium (LDFT) CuO bond length $r_0=2.1$ Å is larger than the cutoff $R=1.6$ Å, the contributions to E_2 become appreciable only at short range. It follows that apart from the Born-Mayer core-overlap contributions, the interface interaction essentially depends, in effect, on the interface ''free volume,'' proportional to the interface separation z. Although Eq. (2) gives a concise parametrization of calculated adhesive energies, its form masks to some extent the qualitative nature of the interface chemical bonding, for example, the dependence of bonding on bond lengths and coordination.

B. Interface electronic structure

The interatomic interactions at the interface are determined fundamentally by the electronic structure, the local electronic spectra and the charge state in the vicinity of the interface are therefore of interest.

1. Interface electronic spectra

LDFT calculations were performed for a bulk interface [(5,6|6) (Mg,O|Cu) layers], a Cu monolayer on an oxygen-terminated MgO substrate, and an unreconstructed oxygen-terminated MgO free surface. Energy spectra for 160 k points were obtained based on the self-consistent electron potential generated with 37 k points. The results were analyzed to determine the layer-projected densities of states in the vicinity of the interface or free surface (see Fig. 3). The densities of states for the layers other than the CuO bilayer at the interface are relatively bulklike, which indicates that the interface perturbation is essentially confined to the interface bilayer. The panels labeled ''bulk'' represent layers two layers removed from the interface. The MgO gap (see second panel from bottom) is approximately 5 eV, considerably smaller than the experimental value of 7.8 eV, as is typical of LDFT calculations. The precise position of the Fermi energy within the MgO gap is determined by the interface dipole potential.

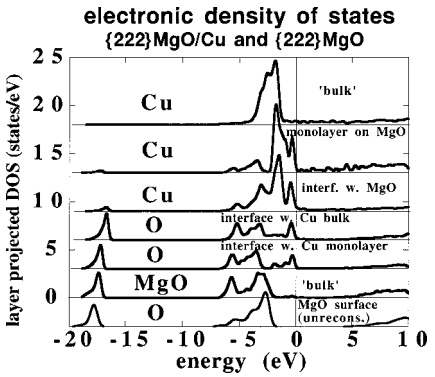

FIG. 3. Calculated layer-projected densities of states for unreconstructed (222) MgO free surface (bottom panel), oxygen-terminated MgO/Cu interface (second, fourth, fifth, and seventh panels), Cu monolayer on oxygen terminated MgO substrate (third and sixth panel) The panels labeled 'bulk' refer to interior layers, two layers away from the interface. The bottom panel was lined up so that the valence band coincides approximately with that in the second panel. The low-lying peak at about -18 eV is the O ($2s$) state.

The densities of states of the interface bilayer (second through fifth panels from the top of Fig. 3) show a peak some tenths of an eV below the Fermi level, within the bulk MgO gap. This peak is absent from the surface O-layer spectrum at an MgO free surface (bottom panel), and results from antibonding hybrid states that mix Cu($3d$) and O($2p$). These are metal-induced gap states, which decay exponentially with distance from the interface.[16] The presence of such high-lying antibonding states of d character (as well as corresponding low-lying bonding states) is typical of copper-oxide bonding and is found, for example, in Cu_2O (Ref. 51) and O/Cu(100) adsorbate systems.[47] Some characteristics of the bonding of these three systems are qualitatively similar, in spite of the differences in their detailed geometries. Oxygen atoms are coordinated to four Cu atoms in Cu_2O and O/Cu(100) and three Cu atoms at an oxygen-terminated coherent {222}MgO/Cu interface. Furthermore, the oxygen-copper bond length in Cu_2O and O/Cu(100) is shorter (1.8–1.9 Å) than for the interface (2.1–2.2 Å), and pd interactions are therefore expected to be somewhat stronger in the former. The tail of the Cu d-band at the interface (second and third panels from the top) extends slightly above the Fermi energy, which opens some d-band holes. The present calculations, however, lack the resolution to determine whether

the interface Cu hole count is enhanced relative to the bulk. Atomic resolution spatially resolved EELS measurements[16] of the $L_{3/2}$ edge did not exhibit any ''white-line'' intensity, which would have been expected in the presence of such enhancement. Since the majority of the Cu-O antibonding states lie within the occupied region, a measurement of these states would be of interest. In principle, this would be possible by x-ray emission[47,48] on an {222}MgO substrate with an evaporated Cu monolayer, although specimen preparation would be difficult because of the instability of free {222}MgO surfaces.[43,49]

2. Interface charge state

In a previous paper,[20] the one-dimensional planar-averaged pseudo-charge density $n(z)$ was analyzed to estimate the charge transferred across the interface relative to free-surface reference systems. As expected, the transfer for oxygen-terminated {222}MgO/Cu polar interfaces, about two tenths of an electron, was greater than that for neutral {100}MgO/Cu interfaces. The geometrical-overlap component of atomic charge transfer,[50] which is added to the physical charge transfer to determine the total charge transfer, however, was not analyzed. The absolute value of charge transfer formulated in this way is somewhat arbitrary and can only be understood by comparison with results for other systems. We have not performed this analysis for MgO/Cu.

Although chemical bonding in bulk MgO is essentially ionic, Cu-O bonding at the interface has characteristics also of covalent and metallic bonding. The incomplete filling of the Cu *d* band gives rise to nonspherical charge densities, directional bonding, and covalency,[51] although these effects are less pronounced at the {222}MgO/Cu interface than in Cu_2O, because of the longer bond lengths. The bonding also has metallic features in view of the nonzero Fermi energy DOS, which is related to metal-induced-gap states.[16] One might naively expect from chemical-valence considerations that both O and Cu adopt their standard charge states $2-$ and $1+$ at the interface, but because of the complex interplay of metallic, ionic, and covalent features at the interface, the formal valences are not in themselves very informative.

IV. SEMICOHERENT INTERFACES

To ascertain the structure and properties of real MgO/Cu interfaces, account must be taken of the large misfit,

$$\eta \equiv (a_{\mathrm{MgO}} - a_{\mathrm{Cu}})/[2(a_{\mathrm{MgO}} + a_{\mathrm{Cu}})] = 0.15. \tag{3}$$

Calculations are performed for two different semicoherent interfaces. The smallest commensurate unit cell consistent with the lattice constant ratio $a_{\mathrm{MgO}}/a_{\mathrm{Cu}} \approx 7/6$ contains 36 MgO and 49 Cu atoms per layer. To simulate an interface with at least three layers on each side would require a unit cell with over three hundred atoms. Although calculations for a cell of this size are not entirely prohibitive, we present here calculations on cells that represent the misfit more approximately.

A. Flat atomic layers

To investigate how the lattice constant mismatch influences the interaction across the interface, we consider a unit cell in which the separations of adjacent Cu atoms along rows in the close packed $[1\bar{1}0]$ direction (parallel to the interface) are shortened, without altering the separation between rows. Specifically, we treat a layer unit cell with 4×1 Cu atoms opposite 3×1 O atoms (Fig. 4). This configuration corresponds to a relative density $\rho = 1.33$, close to the ideal value $\rho = 1.36$. The $4\times1/3\times1$ atomic configuration, although not experimentally realizable, should indicate how the adhesive energy changes for ρ different from unity. The unit cell in this calculation contains 3 MgO and 3 Cu layers, and 30 atoms altogether. The Cu layers below the interface have the same density as the layer at the interface, which ensures that the atomic density on the metallic side of the interface is close to that of bulk Cu. The Cu layers are arranged in an *abc* sequence. As a reference calculation we treat a cell similar to the $4\times1/3\times1$ cell, except that the interface Cu layer is 3×1 and is coherent with the terminating O layer on the MgO side of the interface. In this case a discontinuity in density occurs between the first and second layers of Cu. This reference calculation therefore differs from the coherent interface calculations described in an earlier section, in which no such discontinuity occurs.

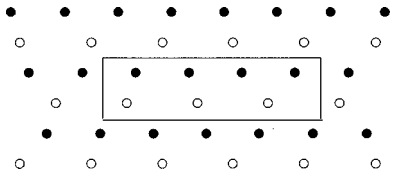

FIG. 4. Small unit-cell model of a semicoherent {222} MgO/Cu interface. Cu interatomic separation along a close-packed direction ($\langle 1\bar{1}0\rangle$, horizontal in figure) is 3/4 that in MgO. Interface unit cell therefore contains 4×1 Cu atoms (closed circles) opposite 3×1 O atoms (open circles).

Calculated total energies as a function of interface spacing for the $4\times1/3\times1$ ($\rho = 1.33$) and the $3\times1/3\times1$ ($\rho = 1.0$) cells were fitted to Eq. (1). We find that the prefactors ϵ (per Cu atom) scaled inversely with the layer atomic density:

$$\rho\epsilon(\rho) = \epsilon(1). \tag{4}$$

Accordingly, no additional interface bonding is achieved by increasing the Cu density beyond the equiatomic composition. (This does not imply that the coherent interface $\rho = 1.0$ is favored, since metal-metal interactions must also be considered.)

The fits to Eq. (1) also yielded $z_0 = 1.49$ (1.30) Å and $l = 0.52$ (0.58) Å for $\rho = 1.33$ (1.0). Although the interface separation z_0 has increased, the mean Cu-O bond length across the interface is about 2.0 Å, close to the value of 2.1 Å corresponding to the coherent interface.

Because of the constraint of flat layers, as well as other approximations, these results must be regarded only as qualitative. To explore the consequences of misfit in more detail, an unconstrained relaxation of the interface must be performed.

B. Fully relaxed atomic layers

Calculations are performed for an interface with layer unit cells of dimension 4×4 (MgO) over 5×5 (Cu). Although

this represents a larger misfit ($\eta=0.22$) than occurs in the actual MgO/Cu interface ($6\times6/7\times7$, $\eta=0.15$), the model calculations are expected to exhibit at least some qualitative features of misfit that are present in the real system. The periodic unit cell comprises 187-atom slabs that consist of 4 layers of O and 3 layers of Mg on the ceramic side and 3 layers of Cu on the metal side. The extra oxygen layer was included to reduce the spurious dipole effect that occurs when an equal number of charged Mg and O layers are employed. The computational cell includes a ''vacuum'' layer (between periodically repeated slabs) with thickness 6.2 Å, analogous to the coherent interface calculations discussed in the preceding section.

It was anticipated that greater relaxation would occur on the metallic side than on the MgO side of the interface, and the lattice constant of Cu was chosen to be 3.56 Å, only about 1% lower than the experimental value. Accordingly, most of the deviation between the misfit of the chosen cell ($\eta=0.22$) and the true system ($\eta=0.15$) is absorbed by the MgO layers. Thus, the lattice constant ratio of 5/4, in conjunction with the Cu lattice constant given above, dictates an MgO lattice constant of 4.45 Å, 6% larger than the experimental value. Since MgO is therefore under a large tensile strain, the relaxation on the MgO side of the interface must be viewed with caution. Calculations for a computational cell that incorporates the true misfit of the system will eliminate the necessity of imposing this unrealistic strain. A calculation for a 399-atom cell is in progress,[42] and the results will be presented elsewhere.

All 187 atoms are allowed to relax both parallel and perpendicular to the interface. To reduce the size of the calculation, optimized Cu and O pseudopotentials[52] were adopted that enable a relatively small plane-wave cutoff energy of 47 Ry, and only the gamma (zone-center) point was used to calculate charge density. The atomic relaxation was accomplished primarily with a quenched molecular dynamics procedure.

The results presented in this work correspond to a starting configuration in which one Cu atom in each unit cell lies precisely in a three-fold hollow site with respect to the interface O layer (Fig. 2). Other parallel translation states could be considered (for example, with one Cu atom per cell in the on-top position), but the chosen one yields the information we are seeking. We note that for a cell with misfit $6\times6/7\times7$ (see Fig. 1 in Ref. 53), with one of the cell dimensions divisible by 3, a cell with one O in an on-top position and another in a threefold hollow site is achieved with the same parallel translation.

1. Mean layer positions and warping

Figure 5 depicts the mean atomic layer coordinate (z) normal to the interface on the abscissa, and the layer warping, represented by the standard deviation of this coordinate for a given layer, on the ordinate. The interface is located at $z=0$, equidistant from the interface Cu and O layers. The mean interface separation is about 1.6 Å, slightly higher but comparable to the value obtained in the flat-atomic-layer calculation presented in the previous section.

The layer warping has a simple interpretation. In well-matched regions, in which the atoms are essentially in hollow sites with respect to their partners across the interface, the layers on both sides of the interface relax towards each other, whereas in poorly matched regions, in which atoms are close to on-top configurations, the layers relax away from each other.

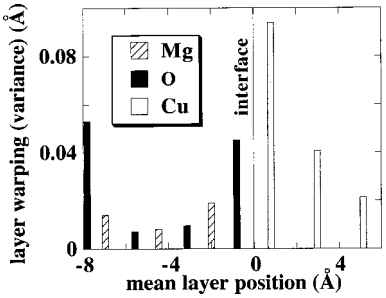

FIG. 5. Layer warping for 187-atom MgO/Cu interface calculation. The abscissa represents the mean value of the coordinate z_i normal to the interface plane for a given atomic layer. The ordinate represents the variance of z_i.

We note that the oxygen layer at the interface shows a warping of about 0.05 Å. It appears reasonable to expect[9] that, because of the stiffer elastic moduli in the ceramic, the atomic-layer relaxation on the MgO side of an MgO/Cu interface would be negligible. This is almost certainly the case for nonpolar interfaces, but some relaxation of the terminating layer in the polar case is plausible because, for example, the oxygen-terminated MgO (111) free surface is thought to be unstable with respect to reconstruction.[43,49,54] Warping of this magnitude (0.05 Å) may still be too small to observe experimentally, for example by high-resolution or Z-contrast electron microscopy.

The layer warping of the ''free-surface'' oxygen layer is larger than that in the interior of the slab. We attribute this strong warping to the tensile strain imposed on the MgO. It does not occur in calculations for unstrained MgO.[42]

2. Interface bond lengths

The forces on the interface Cu and O layers act to optimize the Cu-O bonding across the interface, consistent with the constraints imposed by the local coordination environment. Atoms within the interface bilayer that are situated in regions of good fit (threefold coordination) relax to positions closer to the interface, and those in regions of poor fit (on-top configuration) relax away from the interface, relative to the mean layer coordinate normal to the interface.

The distribution of Cu-O bond lengths across the interface is plotted in Fig. 6, which shows the number of bonds within a bond length interval of 0.1 Å. Three groups of bond lengths may be identified: those in the range 1.9, 2.1, and 2.3 Å. The smallest bond lengths, in the range of 1.9 Å, correspond to essentially on-top Cu-O configurations. This value is close to the Cu-O equilibrium interface separation of 1.8 Å calculated for coherent interfaces with a parallel translation that corresponds to the on-top configuration, as described earlier. The bond lengths in the vicinity of 2.1 Å correspond to atoms close to either threefold hollow sites or twofold bridge sites, and their close partners across the interface. Bonds of nearly on-top or bridge atoms with more distant partners in the layer across the interface are responsible for the bond lengths greater than about 2.3 Å. The average bond length is about

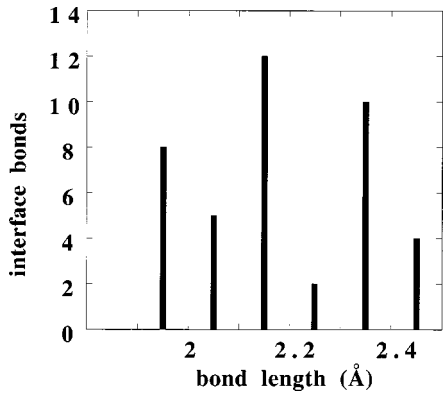

FIG. 6. Distribution of Cu-O bond lengths across interface obtained in 187-atom MgO/Cu interface calculation. The number of bonds per unit cell whose bond lengths fall within intervals of 0.1 Å intervals is shown. Bond lengths of about 1.9 Å correspond to on-top configurations, whereas bond lengths of 2.1 Å correspond to hollow sites or bridge sites.

2.1 Å, close to the equilibrium bond length calculated for coherent interfaces with the parallel translation corresponding to the threefold hollow-site configuration.

3. Misfit dislocations for (111) layers

In Fig. 7 are plotted the atomic coordinates of the Cu-O interface bilayer projected onto the (111) plane of the interface. The unit cell of the calculation, the outline of which is drawn in the figure, is repeated periodically. The figure may be interpreted as a periodic array of regions of good fit (near the centers of the two triangles that make up the diamond-shaped unit cell) interspersed with regions of poor fit (at the corners of the diamond).

The structure of the defect network that results from the superposition of (111) layers has previously been investigated experimentally[53] and by molecular dynamics computer simulation.[55–57] For the relatively small misfit considered in that work, the defect network could be analyzed in terms of misfit dislocations. If the misfit dislocation line segments are perfect dislocations with Burgers vectors of $1/2\langle 110\rangle$ type, the network corresponds to the Wigner-Seitz cell boundaries of a two-dimensional lattice with hexagonal symmetry. When the interface-stacking-fault energy is not too large, however, the nodes of the dislocation network have a tendency to dissociate to reduce the magnitude of the Burgers vectors, at the expense of creating faulted regions. If the dissociation is essentially complete, the dissociated Burgers vectors are of $1/6\langle 211\rangle$ type, and the line segments bound triangular regions with trigonal symmetry.

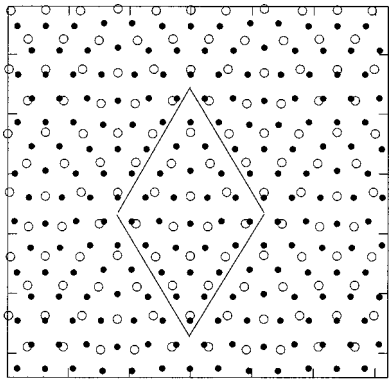

FIG. 7. Cu (filled circles) and O (open circles) interface bilayer atomic positions projected onto a plane parallel to the interface. Boundaries of the diamond shaped unit cell are shown. The cell boundaries connect nodes that represent points of worst match. The upper triangle of the unit cell represents ''normal'' stacking and the lower triangle represents faulted stacking. Based on results of 187-atom MgO/Cu interface calculation. Abscissa is parallel to $\langle 011\rangle$ direction, and ordinate to $\langle 211\rangle$ direction.

The description in terms of misfit dislocations, however, assumes that dislocation core regions may be distinguished from essentially coherent regions. The distinction between dislocation core and regions of good match, however, becomes ambiguous when the mismatch is large and the network cell size is severely reduced. Therefore we do not attempt to quantify rigorously the extent to which dislocations are dissociated. For qualitative discussion, however, it appears natural to regard the lines connecting worst-fitting nodes (on-top sites) as the dislocations, and this gives rise to cells of essentially trigonal symmetry, as observed in atomistic simulations for systems with smaller misfit.[55,56]

V. DISCUSSION

In this work, first-principles calculations are performed for the model interface {222}MgO/Cu. The experimentally relevant oxygen termination is given the most attention, although a few calculations are also performed for the Mg termination. Relatively small unit cells are employed to characterize coherent interfaces, and large-cell calculations are performed to investigate features of the semicoherent interface. Both the coherent and the semicoherent interface calculations have a useful role in the characterization of this interface, as well as other interfaces with large misfit.

Because of the large misfit of {222}MgO/Cu, a realistic simulation of the atomic structure of this system must account for the lattice constant mismatch. Our 187-atom cell calculations provide qualitative information about the atomic relaxation in the presence of misfit. We find that the interface atoms in relatively coherent regions move toward the interface and those in regions of poorer fit move away from it. This occurs on both sides of the interface, and the warping of the O and Cu layers is comparable. The warping of the layers is clearly a property inherent to semicoherent interfaces that is absent in coherent interfaces. We expect these features to persist in calculations that correspond more closely to the true mismatch of {222}MgO/Cu, which are in progress.

Extensive calculations were also performed within the coherent interface approximation. The coherent interface calculations yield interface separations and Cu-O bond lengths across the interface that correspond closely to those found in regions of the semicoherent interfaces where the local environment is similar. For example, the equilibrium interface separation for a coherent interface in the on-top configuration is close to that obtained in the regions of poorest match of the semicoherent interface, where Cu and O atoms are essentially opposite each other. The same correspondence applies to coherent interface calculations in the hollow con-

figuration and regions of best match of the semicoherent interface.

Calculations for coherent interfaces are most suitable for calculating detailed electronic spectra, because extensive *k*-point sampling is required, which is feasible only for small cells. It would be desirable to represent the electronic density of states for the (''true'') semicoherent interface as a superposition of the densities of states obtained for coherent interfaces with different parallel translations. Since the majority of atoms are in regions of relatively good match, it is possible that the results for the hollow-site coherent interface represent, to a good approximation, the spectra for the semicoherent interface. This issue is under investigation and will be discussed elsewhere.

The coherent interface adhesive-energy calculations follow closely the compact analytical representation of Eq. (2). This property will be useful for the design of classical potential models, such as MEAM or variable charge models, for which the satisfaction of Eq. (2) will be a necessary condition. The coherent and semicoherent flat-layer adhesive-energy calculations suggest, see Eq. (4), that the adhesive energies per unit area for the semicoherent interface and the coherent interface are comparable. Further calculations are necessary, however, to confirm this hypothesis.

ACKNOWLEDGMENTS

We thank M. W. Finnis and D. Muller for helpful discussions. R. Benedek and D. N. Seidman were supported at Northwestern University by U.S. Department of Energy Grant No. DEFG02-96ER45597. R.B. acknowledges the hospitality of the Materials Science Division, Argonne National Laboratory. L. H. Yang was supported at Lawrence Livermore National Laboratory by the U.S. Department of Energy under Contract No. W-7405-ENG-48. M. Minkoff was supported at Argonne National Laboratory by the U.S. Department of Energy under Contract No. W-31-109-ENG-38. Most of the computational work was performed at the National Energy Research Supercomputer Center, and at the Argonne National Laboratory SP2 facility.

[1] *Metal-Ceramic Interfaces*, edited by M. Rühle, A. G. Evans, M. F. Ashby, and J. P. Hirth (Pergamon, Oxford, 1990); *Proceedings of the International Symposium on Metal-Ceramic Interfaces*, edited by M. Rühle *et al.* [Acta Metall. Mater. S **40** (1992)]; M. Rühle, J. Surf. Anal. **3**, 157 (1997).

[2] M. W. Finnis, J. Phys.: Condens. Matter **8**, 5811 (1996).

[3] A. Trampert, F. Ernst, C. P. Flynn, H. F. Fischmeister, and M. Rühle, Acta Metall. Mater. **40**, S227 (1992).

[4] A. M. Flank, R. Delaunay, P. Lagarde, M. Pompa, and J. Jupille, Phys. Rev. B **53**, R1737 (1996).

[5] P. Guenard, G. Renaud, and B. Vilette, Physica B **221**, 205 (1996).

[6] H. Jang, D. N. Seidman, and K. L. Merkle, Interface Sci. **1**, 61 (1993).

[7] D. A. Shashkov and D. N. Seidman, Phys. Rev. Lett. **75**, 268 (1995).

[8] P. Lu and F. Cosandey, Ultramicroscopy **40**, 271 (1992); F. R. Chen, S. K. Chiou, L. Chang, and C. S. Hong, *ibid.* **54**, 179 (1994).

[9] W. P. Vellinga and J. Th. M. De Hosson, Mater. Sci. Forum **207-209**, 361 (1996); J. Th. M. De Hosson, W. P. Vellinga, X. B. Zhou, and V. Vitek, in *Stability of Materials*, edited by A. Gonis *et al.* (Plenum, New York, 1996), p. 581; H. B. Groen, B. J. Kooi, W. P. Vellinga, and J. Th. M. De Hosson, Philos. Mag. A **79**, 2083 (1999).

[10] D. K. Chan, D. N. Seidman, and K. L. Merkle, Phys. Rev. Lett. **75**, 1118 (1995).

[11] G. Dehm, M. Rühle, G. Ding, and R. Raj, Philos. Mag. B **71**, 1111 (1995).

[12] S. Köstlmeier, C. Elsässer, B. Meyer, and M. W. Finnis, *Microscopic Simulation of Interfacial Phenomena in Solids and Liquids*, MRS Symposium Proceedings No. 492 (Materials Research Society, Pittsburgh, 1998).

[13] J. Mayer, C. P. Flynn, and M. Rühle, Ultramicroscopy **33**, 51 (1990).

[14] Y. Ikuhara and P. Pirouz, Microsc. Res. Tech. **40**, 206 (1998).

[15] D. A. Shashkov, Ph.D. thesis, Northwestern University, 1997; D. A. Shashkov, M. Chisholm, and D. N. Seidman, Acta Mater. (to be published).

[16] D. A. Muller, D. A. Shashkov, R. Benedek, L. H. Yang, J. Silcox, and D. N. Seidman, Phys. Rev. Lett. **80**, 4741 (1998); Mater. Sci. Forum **294-296**, 99 (1999).

[17] D. Imhoff, S. Laurent, C. Colliex, and M. Backhaus-Ricoult, Eur. Phys. J. A **5**, 9 (1999). The results and conclusions presented by Imhoff, *et al.* differ from those of Muller *et al.* (Ref. 16). These differences may be related to different specimen-preparation procedures as well as the different spatial resolution of the instruments employed by the two groups.

[18] M. Backhaus-Ricoult and S. Laurent, Mater. Sci. Forum **295-296**, 173 (1999); S. Laurent, D. Imhoff, C. Colliex, M. J. Hÿtch, J. Devaud, S. Hagòge, and M. Backhaus-Ricoult, *ibid.* **294-296**, 325 (1999), note that the MgO precipitate morphology varies with the oxygen activity.

[19] J. Goniakowski, Phys. Rev. B **57**, 1935 (1998).

[20] R. Benedek, M. Minkoff, and L. H. Yang, Phys. Rev. B **54**, 7697 (1996).

[21] C. Noguera and G. Bordier, J. Phys. (Paris) **4**, 1851 (1994).

[22] G. Bordier and C. Noguera, Phys. Rev. B **44**, 6361 (1991).

[23] D. M. Lipkin, J. N. Israelachvili, and D. R. Clarke, Philos. Mag. A **76**, 715 (1997).

[24] A. M. Stoneham and P.W. Tasker, J. Phys. C **18**, L543 (1985).

[25] D. M. Duffy, J. H. Harding, and A. M. Stoneham, Acta Metall. Mater. **43**, 1559 (1995).

[26] M. W. Finnis, Acta Metall. Mater. **43**, S25 (1992).

[27] J. Purton, S. C. Parker, and D. W. Bullett, J. Phys.: Condens. Matter **9**, 5709 (1997); J. A. Purton, D. M. Bird, S. C. Parker, and D. W. Bullett, J. Chem. Phys. **110**, 8090 (1999).

[28] J. E. Angelo and M. I. Baskes, Interface Sci. **4**, 47 (1996).

[29] F. H. Streitz and J. W. Mintmire, Phys. Rev. B **50**, 11 996 (1994).

[30] V. Vitek, G. Gutekunst, J. Mayer, and M. Rühle, Philos. Mag. A **71**, 1291 (1995).

[31] R. O. Jones and O. Gunnarsson, Rev. Mod. Phys. **61**, 689 (1989).

[32] M. P. Teter, M. Payne, and D. G. Allan, Phys. Rev. B **40**, 12 255 (1989).

[33] R. Benedek, L. H. Yang, C. Woodward, and B. I. Min, Phys. Rev. B **45**, 2607 (1992).
[34] FEMD is a parallel pseudopotential plane-wave program based on a preconditioned Krylov-space, iterative diagonalization method [see A. Alavi, J. Kohanoff, M. Parrinello, and D. Frenkel, Phys. Rev. Lett. **73**, 2599 (1994)]. The code has been built from CPMD V3.0, developed by J. Hutter *et al.* at IBM Research.
[35] N. Troullier and J. L. Martins, Phys. Rev. B **43**, 1993 (1991).
[36] C. L. Fu and K. M. Ho, Phys. Rev. B **28**, 5480 (1983).
[37] H. Monkhorst and J. D. Pack, Phys. Rev. B **13**, 5188 (1976).
[38] C. Kruse, M. W. Finnis, J. S. Lin, V. Y. Milman, M. C. Payne, A. DeVita, and M. J. Gillan, Philos. Mag. Lett. **73**, 377 (1996).
[39] C. Berthod, J. Bardi, N. Binggeli, and A. Baldereschi, J. Vac. Sci. Technol. B **14**, 3000 (1996).
[40] G. Pacchioni and N. Rösch, J. Chem. Phys. **104**, 7329 (1996); I. Yudanov, G. Pacchioni, K. M. Neyman, and N. Rösch, J. Phys. Chem. B **101**, 2786 (1997); A. V. Matveev, K. M. Neyman, I. V. Yudanov, and N. Rösch, Surf. Sci. **426**, 123 (1999).
[41] J. P. Perdew *et al.*, Phys. Rev. B **46**, 6671 (1992).
[42] R. Benedek, A. Alavi, D. N. Seidman, L. H. Yang, D. A. Muller, and C. Woodward (unpublished).
[43] R. Plass, K. Egan, C. Collazo-Davila, D. Grozea, E. Landree, L. D. Marks, and M. Gajdardziska-Josifovska, Phys. Rev. Lett. **81**, 4891 (1998).
[44] T. Hong, J. R. Smith, and D. J. Srolovitz, J. Adhes. Sci. Technol. **8**, 837 (1994).
[45] J. R. Smith, T. Hong, and D. J. Srolovitz, Phys. Rev. Lett. **72**, 4021 (1994).
[46] J. Tersoff, Phys. Rev. Lett. **56**, 632 (1986).
[47] T. Wiell, J. E. Klepeis, P. Bennich, O. Björneholm, N. Wassdahl, and A. Nilsson, Phys. Rev. B **58**, 1655 (1998).
[48] P. Jonnard, C. Hombourger, F. Vergand, C. Bonnelle, B. Ealet, A. Renou, and E. Gillet, Surf. Rev. Lett. **5**, 369 (1998).
[49] A. Pojani, F. Finocchi, J. Goniakowski, and C. Noguera, Surf. Sci. **54**, 7697 (1997).
[50] R. Benedek, A. P. Smith, and L. H. Yang, Phys. Rev. B **49**, 7786 (1994).
[51] P. Marksteiner, P. Blaha, and K. Schwarz, Z. Phys. B **64**, 119 (1986).
[52] J.S. Lin, A. Qteish, M. C. Payne, and V. Heine, Phys. Rev. B **47**, 4174 (1993).
[53] F. Ernst, Philos. Mag. A **68**, 1251 (1993).
[54] M. Baudin, M. Wojcik, and K. Hermansson, Surf. Sci. **375**, 374 (1997).
[55] C. M. Gilmore, Phys. Rev. B **40**, 6402 (1989).
[56] M. Dornheim and H. Teichler, Phys. Status Solidi **171**, 267 (1999).
[57] L. A. Zepeda-Ruiz, D. Maroudas, and W. H. Weinberg, J. Appl. Phys. **85**, 3677 (1999).